Methods to Suppress Power Oscillation Caused by Disharmonized Voltage-source-controlled Units at Both Sides of Transmission Line

Qiyi Yu and Yi Tang, *Senior Member*, *IEEE*

***Abstract*—Previous studies have demonstrated that disharmony among voltage-source-controlled units may occur on an AC transmission or distribution line under steady-state operating conditions or quasi-static operating conditions. To prevent disharmony oscillations from threatening the secure and stable operation of power grids, two novel disharmony oscillation suppression (DOS) methods are proposed in this paper. First, the oscillation characteristics of single-phase instantaneous current and power under disharmony operating conditions are investigated. The key parameters and typical indicators for monitoring disharmony oscillations, such as disharmony frequency and average power, are listed. Second, two DOS strategies are designed based on directly monitoring the frequency difference and indirectly monitoring line power, respectively. Finally, the characteristics of disharmony oscillations are thoroughly analyzed through a case study, and the proposed DOS strategies are validated in simulations using MATLAB/Simulink.**

***Index Terms*—New-type power system, disharmony oscillation, power oscillation suppression, disharmony, voltage-source-controlled unit.**

I. Introduction

Grid-forming (GFM) converter and new energy generation technologies are becoming more mature. The number of voltage-sourced grid-connected units is increasing in new-type power systems (NTPS), such as high voltage direct current (HVDC) transmission systems and energy storage based on GFM converters [1]–[3]. The output characteristics of the grid-connected unit described above depend on GFM converters. Its instability problems are a serious threat to the safe operation of power grids. So far, research has been mainly focused on such problems, which can be divided into two categories: small-signal instability problems and large-signal instability problems.

Small-signal instability can be classified into low-frequency oscillation (LFO), subsynchronous oscillation (SSO), and high-frequency oscillation (HFO). LFO may be induced by factors such as the conventional matching control [4] in photovoltaic systems, multiloop control [5] in modular multilevel converter (MMC)-based HVDC, and the constant power dynamics at the DC link [6]. Reference [7] reveals that LFO may easily occur owing to DC-link voltage synchronization and phase lag introduced by voltage and current dual close loop control. LFO suppression methods include but are not limited to power system stabilizer [8], phase compensation [9], active-damping control [10], and optimizing control parameters [11]. SSO may occur in strong grids [12] and the series-compensated grid-connected systems [13], [14], which is related to the impedance of inverter and the natural resonance frequency of the grid impedance, respectively. In [15], it is reported that SSO is induced by interactions between GFM converters of a bipolar HVDC link. SSO suppression methods include but are not limited to virtual impedance [16], [17] and active damping control [18]. For HFO, it is mainly related to time delay of MMC-based HVDC [19]. Meanwhile, terminal voltage feedforward control, voltage-frequency control, and grid current control have a great effect on the negative damping region [20]. HFO suppression methods include but are not limited to reducing the control delay [19], [20], adding a low-pass filter in the outer loop control proportion path [21], and virtual impedance method [22].

The large-signal instability can be divided into two categories [23]: large-signal instability with equilibrium points and without any equilibrium points. Whether the two types of instability problems occur or not depends on the fault type, the power angle characteristics of the GFM converter, and the synchronization dynamics [24]. Among them, the power angle characteristics and the synchronization dynamics are related to the current limiters [25] and the synchronization control structure [26]. Based on the instability mechanism, the methods to improve transient stability can be divided into two categories: 1) changing the power reference; 2) modifying control loops or controller parameters. For the

Received: November 18, 2024
Accepted: July 25, 2025
Published Online: November 1, 2025
Qiyi Yu and Yi Tang (corresponding author) are with the School of Electrical Engineering, Southeast University, Nanjing 210018, China (e-mail: yqypaper@126.com; tangyi@seu.edu.cn).
DOI: 10.23919/PCMP.2024.000383

former, the transient stability can be enhanced by adaptively adjusting the active power [27] and rejecting reactive power [28]. For the latter, the problems are solved by introducing transient switched operation mode [29], improving the current limiting control [30], [31], optimizing the reactive-voltage control loop [32], employing adaptive inertia and damping parameters [33], [34], and employing virtual power angle limiting method [35].

Most of the above studies focus on analyzing the phase instability of GFM converters. Stability enhancement methods are proposed from the aspects of internal parameters and control characteristics. The reviewed literature maintains three critical assumptions: 1) neglecting the minor differences in output frequencies of GFM converters at different nodes under steady-state operating conditions (SSOCs) or quasi-static operating conditions (QSSOCs); 2) assuming that the frequency of each node can be quickly restored to a specified level after a disturbance; and 3) assuming identical frequency measurement and control errors of GFM converters at different nodes. Revisiting the aforementioned assumptions will give rise to the following new questions.

The differences in both frequency measurement errors and control errors among GFM converters result in weak frequency-harmonization ability of these converters without coordinated synchronization mechanisms. Meanwhile, massive converter integration into NTPS weakens the phase-synchronization ability of NTPS. Thus, a new problem called disharmony will occur owing to weak frequency-harmonization ability and phase-synchronization ability, thereby exhibiting operational characteristics distinct from those in 1) and 2). The authors concludes in our previous studies [36], [37] that the disharmony phenomenon occurs in NTPS under SSOCs or QSSOCs. This disharmony phenomenon manifests as inconsistency in the output frequencies of GFM converters and other voltage-source converter units (VSCUs) at both ends of the AC transmission line for a longer period. The frequency difference between the VSCU output frequency and the power frequency (50 Hz or 60 Hz) is minimal, typically not exceeding 0.01 Hz in magnitude [38]. This disharmony phenomenon can induce long-period oscillations at the grid side called disharmony oscillations. The power grid of the former Soviet Union experienced similar oscillation issues, including unregulated power oscillations with an average period of up to 1 hour, and long-period oscillations and resonance due to asynchronous operation [39]. It is not conducive to the secure and stable operation of power grids. Therefore, it is necessary to study the suppression strategy. This paper analyzes the disharmony oscillation caused by disharmonized VSCUs, including characteristics and disharmony oscillation suppression (DOS) methods. The main contributions of this paper are as follows.

1) This paper provides the first comprehensive characteristics of grid-side disharmony oscillation induced by two disharmonized VSCUs, which helps explain long-period oscillation phenomena in power grids that align with the definition of disharmony oscillation.

2) The key parameters and typical indicators under disharmony operating conditions (DOCs) are identified to monitor disharmony oscillation.

3) This paper proposes novel methods to address disharmony oscillations, including respective DOS strategies based on directly monitoring the frequency difference and indirectly monitoring line power.

This paper is organized as follows. Section II elaborates on the equivalent model of an AC transmission line with two VSCUs and analyzes current and power characteristics under DOCs. Section III summarizes characteristic indicators for monitoring the disharmony oscillation and proposes DOS strategies. Section IV presents the case study and analysis results, and Section V concludes this paper.

II. Mechanism Analysis of Oscillation of Disharmonized VSCUs

A. Equivalent Circuit Model of AC Transmission Line with Disharmonized VSCUs

The disharmony oscillations originate from disharmony between two VSCUs, indicating that it is a localized grid issue. Meanwhile, considering that disharmony occurs under SSOCs or QSSOCs, each VSCU is modeled as a controlled voltage source (CVS) and an equivalent circuit model is established in Fig. 1. Schemes of active power oscillation suppression under DOCs and critical parameters of the equivalent circuit model are shown in Fig. 1 and Table I, respectively.

TABLE I
Parameters of the Equivalent Circuit Model

Location	Parameter	Value
$VSCU_s$	Single-phase root-mean-square voltage U_s (p.u.)	1.050
	Initial phase φ_s (°)	10.00
	Frequency f_s (Hz)	49.99
$VSCU_r$	Single-phase root-mean-square voltage U_r (p.u.)	1.010
	Initial phase φ_r (°)	0.00
	Frequency f_r (Hz)	50.01
Transmission line	Length of line (km)	290
	Resistance of unit-length line r_0 (Ω/km)	0.023 543
	Inductance of unit-length line l_0 (mH/km)	0.860 016
	Capacitance of unit-length line c_0 (μF/km)	0.013 100
	Base value of three phase phase-to-line voltage (kV)	500
	Fundamental frequency f_b (Hz)	50
Transfer function parameters	Gain K_f	1.0
	Time constant T_f (s)	0.02

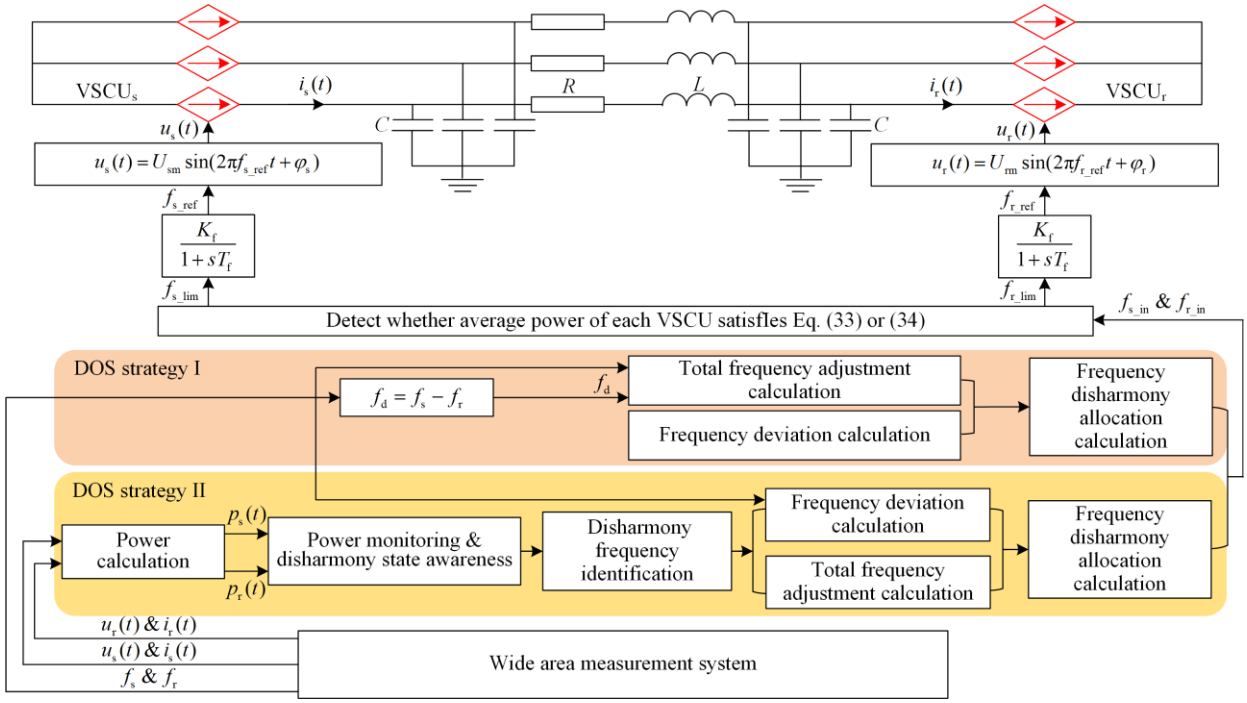

Fig. 1. The equivalent circuit model of AC transmission line with two VSCUs and schemes of active power oscillation suppression under DOCs.

In Fig. 1, $u_s(t)$, $u_r(t)$, $i_s(t)$ and $i_r(t)$ are the single-phase instantaneous voltages and current of VSCU$_s$ and VSCU$_r$, respectively; R, L, and C are the single-phase resistance, inductance, and ground capacitance of line, respectively; f_{s_in} and f_{r_in} are the frequencies of VSCU$_s$ and VSCU$_r$ from active power oscillation suppressors; f_{s_lim} and f_{r_lim} are the frequencies of VSCU$_s$ and VSCU$_r$ after detection; and the transfer function $K_f/(1+sT_f)$ simulates the internal control loop regulation characteristics of VSCUs.

Under SSOCs or QSSOCs, the output voltage and frequency of each VSCU can be temporarily regarded as a constant value for a duration that is bigger than or equal to the disharmony period. Accordingly, $u_s(t)$ and $u_r(t)$ can be expressed as:

$$u_s(t)=U_{sm}\sin(\omega_s t+\varphi_s) \tag{1}$$

$$u_r(t)=U_{rm}\sin(\omega_r t+\varphi_r) \tag{2}$$

where U_{sm} and U_{rm} are the maximum values of $u_s(t)$ and $u_r(t)$, respectively; ω_s and ω_r are the angular frequencies with the corresponding frequency denoted by f_s and f_r, respectively; φ_s and φ_r are the initial phase of $u_s(t)$ and $u_r(t)$, respectively.

To measure the degree of disharmony between two VSCUs, the disharmony angular frequency ω_d and the corresponding disharmony period T_d are:

$$\omega_d=\omega_s-\omega_r \tag{3}$$

$$T_d=\frac{1}{|f_s-f_r|} \tag{4}$$

In real power grids, ω_d is not exactly equal to 0 rad/s due to distributed synchronous GFM mode and disharmony factors [34], [35]. To avoid this oscillation problem threatening the secure and stable operation of power grids, we will analyze the main characteristics of disharmony oscillations and propose DOS strategies later.

B. Mechanism Analysis of Line Current

The equivalent circuit in Fig. 1 is a linear circuit, so the superposition theorem can be applied to derive $i_s(t)$. When frequency is f_s or f_r, the single-phase current phasorr $\dot{I}_{s(s)}$ and $\dot{I}_{s(r)}$ can be written respectively as:

$$\dot{I}_{s(s)}=\dot{U}_s(\omega_s)\left[\mathrm{j}\omega_s C+1/\left(R+\mathrm{j}\omega_s L\right)\right]=\frac{I_{sm(s)}}{\sqrt{2}}\mathrm{e}^{\mathrm{j}\alpha_s} \tag{5}$$

$$\dot{I}_{s(r)}=-\dot{U}_r(\omega_r)/\left(R+\mathrm{j}\omega_r L\right)=\frac{I_{sm(r)}}{\sqrt{2}}\mathrm{e}^{\mathrm{j}\alpha_r} \tag{6}$$

where $\dot{U}_s(\omega_s)$ and $\dot{U}_r(\omega_r)$ are the single-phase voltage phasors of VSCU$_s$ and VSCU$_r$ with only one CVS at node s or r, respectively; $\frac{I_{sm(s)}}{\sqrt{2}}$, $\frac{I_{sm(r)}}{\sqrt{2}}$, α_s and α_r are the module and angle of the terms, respectively.

Based on (5) and (6), $i_s(t)$, and its peak value $I_{sm}(t)$ and initial phase $\alpha(t)$ can be respectively derived as:

$$i_s(t)=I_{sm}(t)\sin\left[\omega_r t+\alpha(t)\right] \tag{7}$$

$$\begin{cases} I_{sm}(t)=\sqrt{I_{sm(s)}^2+I_{sm(r)}^2+2I_{sm(s)}I_{sm(r)}\cos\left(\omega_d t+\alpha_s-\alpha_r\right)} \\ \alpha(t)=\operatorname{atan2}\left(\begin{matrix} I_{sm(s)}\cos(\omega_d t+\alpha_s)+I_{sm(r)}\cos\alpha_r, \\ I_{sm(s)}\sin(\omega_d t+\alpha_s)+I_{sm(r)}\sin\alpha_r \end{matrix}\right) \end{cases} \tag{8}$$

where function atan2(x, y) is the angle between (x, y) and the positive x-axis.

Based on (3)–(8), the abnormal characteristics of peak value or amplitude of $i_s(t)$ and its initial phase under DOCs and harmony operating conditions (HOCs) are analyzed from the following two aspects.

1) Under DOCs ($\omega_s \neq \omega_r$), $I_{sm}(t)$ and $\alpha(t)$ are both periodic functions whose periods are T_d. The maximum $I_{sm(max)}$ of $I_{sm}(t)$ can be derived from (8) as:

$$I_{sm(max)} = \sqrt{I_{sm(s)}^2 + I_{sm(r)}^2 + 2I_{sm(s)}I_{sm(r)}} = I_{sm(s)} + I_{sm(r)} \quad (9)$$

2) Under HOCs ($\omega_s = \omega_r$), the line current peak $I_{sm}^{[har]}$ and $\alpha(t)$ are constant. $I_{sm}^{[har]}$ can be written as:

$$I_{sm}^{[har]} = \sqrt{\left(I_{sm(s)}^{[har]}\right)^2 + \left(I_{sm(r)}^{[har]}\right)^2 + 2I_{sm(s)}^{[har]}I_{sm(r)}^{[har]}\cos\left(\alpha_s - \alpha_r\right)} \quad (10)$$

where $I_{sm(s)}^{[har]}$ and $I_{sm(r)}^{[har]}$ are obtained from $I_{sm(s)}$ and $I_{sm(r)}$ with $\omega_d = 0$ rad/s.

Further, the current peak gain K_{cp} can be given as:

$$K_{cp} = \frac{I_{sm(max)}}{I_{sm}^{[har]}} \quad (11)$$

K_{cp} is the key indicator that assesses the oscillation amplification effect of line current peak values before and after disharmony. The larger K_{cp} is, the more seriously the line current will be influenced by the disharmonized VSCUs, implying a more severe disharmony.

C. Mechanism Analysis of Line Power Under DOCs

In this subsection, the characteristics of line power will be analyzed in terms of instantaneous power and average power.

1) Single-phase Instantaneous Power

Multiplying (1) by (7) yields instantaneous power $p_s(t)$ at node s as:

$$p_s(t) = 0.5U_{sm}I_{sm}(t) \times \begin{bmatrix} \cos\left(\omega_d t + \varphi_s - \alpha(t)\right) - \\ \cos\left((\omega_d + 2\omega_r)t + \varphi_s + \alpha(t)\right) \end{bmatrix} \quad (12)$$

As shown in (12), $p_s(t)$ consists of two terms. The first term is a long-period component and the second term is a short-period component.

Based on (12), the abnormal characteristics of peak value of $p_s(t)$ under DOCs and HOCs are analyzed from the following two aspects.

1) Under DOCs ($\omega_s \neq \omega_r$), the upper and lower envelopes of $p_s(t)$ can be derived by keeping the long-period term and setting $-\cos\left[\left(\omega_d + 2\omega_r\right)t + \varphi_s + \alpha\left(t\right)\right]$ to ± 1 in (12). They are denoted as $p_{s\text{-}env}^{[upp]}(t)$ and $p_{s\text{-}env}^{[low]}(t)$, respectively:

$$\begin{cases} p_{s\text{-}env}^{[upp]}(t) \approx 0.5U_{sm}I_{sm}(t) \times \left[\cos\left(\omega_d t + \varphi_s - \alpha(t)\right) + 1\right] \\ p_{s\text{-}env}^{[low]}(t) \approx 0.5U_{sm}I_{sm}(t) \times \left[\cos\left(\omega_d t + \varphi_s - \alpha(t)\right) - 1\right] \end{cases} \quad (13)$$

where $p_{s\text{-}env}^{[upp]}(t)$ and $p_{s\text{-}env}^{[low]}(t)$ are both periodic functions whose periods are T_d. The maximum value $P_{s\text{-}env(max)}^{[upp]}$ of $p_{s\text{-}env}^{[upp]}(t)$ and the minimum value $P_{s\text{-}env(min)}^{[low]}$ of $p_{s\text{-}env}^{[low]}(t)$ can be obtained according to (13).

2) Under HOCs ($\omega_s = \omega_r$), the single-phase instantaneous line power $p_s^{[har]}(t)$ at node s can be derived from (12) as:

$$p_s^{[har]}(t) = 0.5U_{sm}I_{sm}^{[har]} \times \begin{bmatrix} \cos\left(\varphi_s - \alpha^{[har]}\right) - \\ \cos\left(2\omega t + \varphi_s + \alpha^{[har]}\right) \end{bmatrix} \quad (14)$$

where initial phase $\alpha^{[har]}$ of $p_s(t)$ under HOCs is:

$$\alpha^{[har]} = \operatorname{atan2}\begin{pmatrix} I_{sm(s)}^{[har]}\cos\alpha_s + I_{sm(r)}^{[har]}\cos\alpha_r, \\ I_{sm(s)}^{[har]}\sin\alpha_s + I_{sm(r)}^{[har]}\sin\alpha_r \end{pmatrix} \quad (15)$$

The peak value of $p_s(t)$ under HOCs can be obtained by (14) as:

$$P_{s\,max}^{[har]} = 0.5U_{sm}I_{sm}(t) \times \left[\cos(\varphi_s - \alpha) + 1\right] \quad (16)$$

Further, the power peak gain K_{pp} can be given as:

$$K_{pp} = \frac{P_{s\text{-}env(max)}^{[upp]}}{P_{s\,max}^{[har]}} \quad (17)$$

K_{pp} is the key indicators that assess the amplification effect of power oscillation before and after disharmony. The larger K_{pp} is, the more seriously the disharmonized VSCUs will influence the line power, implying more severe disharmony.

2) Power Factor Angle

Let ω_r be the angular frequency reference, the single-phase current phasor $\dot{I}_s(t)$ and voltage phasor $\dot{U}_s(t)$ can be derived by (7) and (1) as:

$$\dot{I}_s(t) = I_s(t)\mathrm{e}^{\mathrm{j}\alpha(t)} \quad (18)$$

$$\dot{U}_s(t) = U_s\,\mathrm{e}^{\mathrm{j}(\omega_d t + \varphi_s)} \quad (19)$$

where $I_s(t)$ is the amplitude of the single-phase current phasor whose period is T_d; and U_s is the amplitude of the single-phase voltage phasor.

The power factor angle $\theta(t)$, lagging angle between $\dot{I}_s(t)$ and $\dot{U}_s(t)$ can be derived from (18) and (19) as:

$$\theta(t) = \omega_d t + \varphi_s - \alpha(t) \quad (20)$$

The remainder function mod ($\theta(t)$, 2π) from a division of $\theta(t)$ by 2π is a periodic function whose period is T_d.

Further, the complex power $S_s(t)$ and active power $P_s(t)$ can be expressed respectively as:

$$S_s(t) = U_s I_s(t) e^{j\theta(t)} \quad (21)$$

$$P_s(t) = U_s I_s(t) \cos\theta(t) \quad (22)$$

Equation (22) shows that: 1) $P_s(t)$ is a periodic function whose period is T_d; and 2) Due to the periodicity of $\theta(t)$, $P_s(t)$ is positive or negative in a disharmony period. During the disharmony period, the delivery direction of $P_s(t)$ is positive for a portion of the time and negative for the remainder.

III. Proposed DOS Strategies

A. Key Indicators for Monitoring Disharmony Oscillation

Based on Sections II, Appendix A and B, the characteristics of disharmony oscillations are given below.

1) Disharmony oscillations are long-period oscillations at power grid side and $|f_d| \leqslant 0.02$ Hz in general.

2) $I_{sm}(t)$ and $\alpha(t)$ are both periodic functions whose periods are T_d.

3) $p_{s\text{-}env}^{[upp]}(t)$ and $p_{s\text{-}env}^{[low]}(t)$ are both periodic functions whose periods are T_d.

4) The remainder from a division of $\theta(t)$ by 2π is a periodic function whose period is T_d.

5) $P_s(t)$ is a periodic function whose period is T_d.

6) During the disharmony period, the delivery direction of $P_s(t)$ is positive for a portion of the time and negative for the remainder.

7) The average value of $p_s(t)$ is equal to the average value of $P_s(t)$ during a disharmony period.

In summary, the condition for the occurrence of disharmony oscillations in transmission lines is that ω_d remains non-zero over a prolonged duration.

Based on the above characteristics of disharmony oscillations, there are several ways to monitor whether disharmony oscillations occur as follows.

1) Monitor whether ω_d or frequency difference is non-zero for a long time.

2) Monitor whether $I_{sm}(t)$, $\alpha(t)$, $\theta(t)$, $p_{s\text{-}env}(t)$, and $P_s(t)$ deviate from the corresponding values under HOCs and have long periodic oscillations in their neighborhood.

3) Monitor whether the ratio of the peak current to $I_{sm}^{[har]}$ or the ratio of the peak power to $P_{smax}^{[har]}$ exceeds the limit.

4) Monitor whether the ratio of $P_s(t)$ to the average value of $p_s(t)$ over a fundamental cycle under HOCs exceeds the limit.

5) Monitor whether the delivery direction of the average value of $p_s(t)$ over a fundamental cycle is reversed.

6) Monitor whether $P_s(t)$ or the average value of $p_s(t)$ over a fundamental frequency cycle deviates from the setting threshold.

In the following section, the DOS strategies based on directly monitoring the frequency difference and indirectly monitoring line power will be proposed in terms of 1) and 6) of the above monitoring means, respectively. Ideas for DOS based on multiple means will also be provided.

B. DOS Strategy

In this section, DOS schemes are designed, including DOS strategies based on one single and multiple means. In the process of strategic decision-making, the top-level control center is responsible for centralized computation and decision-making, and dispatching frequency instructions to VSCUs, or transmitting computation information to assist the VSCUs in distributed computation and decision-making. DOS strategies are as follows.

1) DOS Strategy Based on One Single Means

a) DOS Strategy I: Control Strategy Based on Directly Monitoring Frequency Difference

Figure 2 shows the scheme of DOS strategy I which consists of four parts.

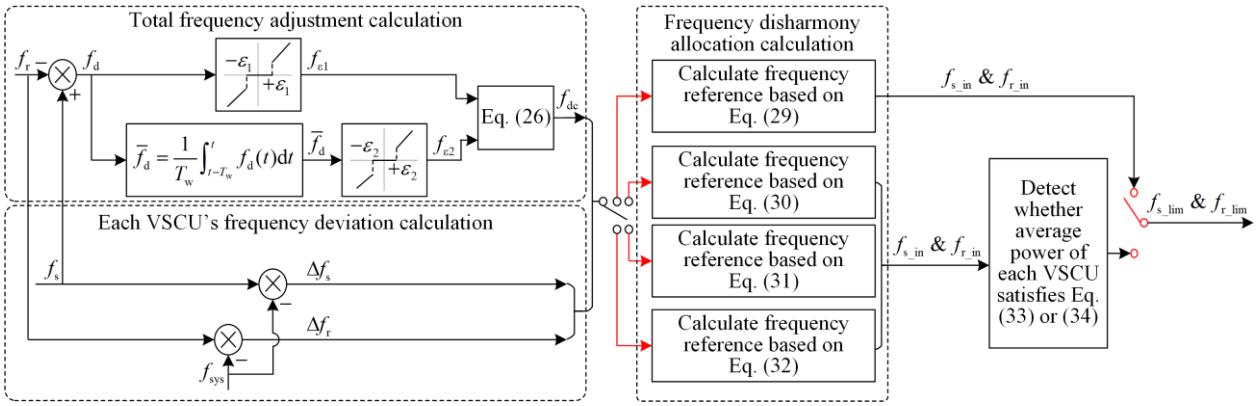

Fig. 2. DOS based on the frequency difference.

Part 1 is about the total frequency adjustment calculation.

First, disharmony frequency f_{d} and its average value $\overline{f}_{\mathrm{d}}$ are obtained based on f_{r} and f_{s} from wide area measurement system, as:

$$\begin{cases} f_{\mathrm{d}} = f_{\mathrm{s}} - f_{\mathrm{r}} \\ \overline{f}_{\mathrm{d}} = \dfrac{1}{T_{\mathrm{w}}} \displaystyle\int_{t-T_{\mathrm{w}}}^{t} f_{\mathrm{d}} \mathrm{d}t \end{cases} \tag{23}$$

where T_{w} is generally several times the length of a fundamental cycle due to long-period property of disharmony oscillation.

Second, detect whether f_{d} and its average value $\overline{f}_{\mathrm{d}}$ have reached the corresponding threshold values under DOCs. The setting $f_{\varepsilon 1}$ of f_{d}, and the setting $f_{\varepsilon 2}$ of $\overline{f}_{\mathrm{d}}$ are obtained respectively as:

$$f_{\varepsilon 1} = \begin{cases} 0, & \left|f_{\mathrm{d}}\right| \leqslant \varepsilon_1 \\ f_{\mathrm{d}}, & \left|f_{\mathrm{d}}\right| > \varepsilon_1 \end{cases} \tag{24}$$

$$f_{\varepsilon 2} = \begin{cases} 0, & \left|\overline{f}_{\mathrm{d}}\right| \leqslant \varepsilon_2 \\ \overline{f}_{\mathrm{d}}, & \left|\overline{f}_{\mathrm{d}}\right| > \varepsilon_2 \end{cases} \tag{25}$$

where ε_1 is the threshold value of f_{d} and ε_2 is the threshold value of $\overline{f}_{\mathrm{d}}$. Generally, each threshold is an order of magnitude smaller than the value given in Section III.A.

Finally, the total frequency adjustment f_{dc} is determined as:

$$f_{\mathrm{dc}} = \begin{cases} w_1 f_{\varepsilon 1} + w_1 f_{\varepsilon 2}, & f_{\varepsilon 1} f_{\varepsilon 2} \neq 0 \text{ and } w_1 + w_2 = 1 \\ 0, & f_{\varepsilon 1} f_{\varepsilon 2} = 0 \end{cases} \tag{26}$$

where w_1 and w_2 are the weighting coefficients of $f_{\varepsilon 1}$ and $f_{\varepsilon 2}$, respectively, and generally, $w_1 = w_2 = 0.5$.

This part prevents the frequency difference detection from being affected by random noise.

Part 2 is about each VSCU's frequency deviation calculation.

To determine the VSCUs involved in frequency regulation, the difference Δf_{s} between the output frequency of $\mathrm{VSCU_s}$ and the power grid frequency, and the difference Δf_{r} between the output frequency of $\mathrm{VSCU_s}$ and the power grid frequency are calculated as:

$$\Delta f_{\mathrm{s}} = f_{\mathrm{s}} - f_{\mathrm{sys}} \tag{27}$$

$$\Delta f_{\mathrm{r}} = f_{\mathrm{r}} - f_{\mathrm{sys}} \tag{28}$$

where f_{sys} is the frequency signal acquired from measurement system or the frequency reference issued by the regional AC power grid control center which is generally equal to the fundamental frequency.

Part 3 is about the frequency disharmony allocation calculation.

Based on Δf_{s} and Δf_{r}, the frequency disharmony allocation is determined, which is mainly divided into the following four cases.

Case 1: $\Delta f_{\mathrm{s}} \neq 0$, $\Delta f_{\mathrm{r}} \neq 0$, $f_{\mathrm{dc}} = 0$. When $\mathrm{VSCU_s}$ and $\mathrm{VSCU_r}$ are harmonized but each VSCU and its corresponding AC power grid are disharmonized, the output frequencies of each VSCU need to be adjusted. The frequency $f_{\mathrm{s\_in}}$ of $\mathrm{VSCU_s}$ and frequency $f_{\mathrm{r\_in}}$ of $\mathrm{VSCU_r}$ for instruction are as follows:

$$\begin{cases} f_{\mathrm{s\_in}} = f_{\mathrm{sys}} \\ f_{\mathrm{r\_in}} = f_{\mathrm{sys}} \end{cases} \tag{29}$$

Case 2: $\Delta f_{\mathrm{s}} \neq 0$, $\Delta f_{\mathrm{r}} = 0$, $f_{\mathrm{dc}} \neq 0$. When $\mathrm{VSCU_r}$ and AC power grid at the receiving end are harmonized but $\mathrm{VSCU_r}$ and $\mathrm{VSCU_s}$ are disharmonized, only the output frequency of $\mathrm{VSCU_s}$ needs to be adjusted. The frequency $f_{\mathrm{s\_in}}$ of $\mathrm{VSCU_s}$ and frequency $f_{\mathrm{r\_in}}$ of $\mathrm{VSCU_r}$ for instruction are as follows:

$$\begin{cases} f_{\mathrm{s\_in}} = f_{\mathrm{s}} - f_{\mathrm{dc}} \\ f_{\mathrm{r\_in}} = f_{\mathrm{r}} \end{cases} \tag{30}$$

Case 3: $\Delta f_{\mathrm{s}} = 0$, $\Delta f_{\mathrm{r}} \neq 0$, $f_{\mathrm{dc}} \neq 0$. When $\mathrm{VSCU_s}$ and AC power grid at the sending end are harmonized but $\mathrm{VSCU_r}$ and $\mathrm{VSCU_s}$ are disharmonized, only the output frequency of $\mathrm{VSCU_r}$ needs to be adjusted. The frequency $f_{\mathrm{s\_in}}$ of $\mathrm{VSCU_s}$ and frequency $f_{\mathrm{r\_in}}$ of $\mathrm{VSCU_r}$ for instruction are as follows:

$$\begin{cases} f_{\mathrm{s\_in}} = f_{\mathrm{s}} \\ f_{\mathrm{r\_in}} = f_{\mathrm{r}} + f_{\mathrm{dc}} \end{cases} \tag{31}$$

Case 4: $\Delta f_{\mathrm{s}} \neq 0$, $\Delta f_{\mathrm{r}} \neq 0$, $f_{\mathrm{dc}} \neq 0$. When $\mathrm{VSCU_s}$, $\mathrm{VSCU_r}$ and AC power grid at the sending and receiving ends are disharmonized, the output frequencies of $\mathrm{VSCU_s}$ and $\mathrm{VSCU_r}$ need to be adjusted. The frequency $f_{\mathrm{s\_in}}$ of $\mathrm{VSCU_s}$ and frequency $f_{\mathrm{r\_in}}$ of $\mathrm{VSCU_r}$ for instruction are as follows:

$$\begin{cases} f_{\mathrm{s\_in}} = f_{\mathrm{s}} - \dfrac{\Delta f_{\mathrm{s}}}{\left|\Delta f_{\mathrm{s}}\right| + \left|\Delta f_{\mathrm{r}}\right|} \left|f_{\mathrm{dc}}\right| \\ f_{\mathrm{r\_in}} = f_{\mathrm{r}} - \dfrac{\Delta f_{\mathrm{r}}}{\left|\Delta f_{\mathrm{s}}\right| + \left|\Delta f_{\mathrm{r}}\right|} \left|f_{\mathrm{dc}}\right| \end{cases} \tag{32}$$

Part 4 is about the frequency control instruction transmission.

Over long time scales, precise control is impeded by measurement uncertainties and system control errors. After the frequency control instructions are executed by each VSCU, the power flow may temporarily recover from the disharmony state to the harmony state or its corresponding neighborhoods. However, over time, the power flow gradually deviates from the normal state due to slight disharmony or new disharmony problem, eventually driving the system into a new disharmony state. Consequently, it is necessary to issue new frequency control instructions to each VSCU before the power flow exceeds the limit to correct the direction and magnitude of the flow deviation. A scheme for serialized monitor and control based on average power under DOCs is proposed in Fig. 3.

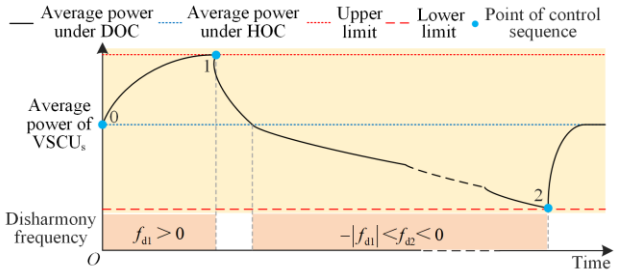

Fig. 3. Scheme for serialized monitor and control based on $P_s(t)$.

Take $P_s(t)$ as the monitor signal and assume that disharmony occurs at point 0 of the control sequence and the disharmony frequency is f_{d1} in Fig. 3. Only the average power is monitored continually, if $P_s(t)$ does not exceed the setting upper limit $P_{s\text{-upl}}$ or lower limit $P_{s\text{-lowl}}$ of average power. When $P_s(t)$ approaches the setting power limit, a new frequency control instruction is sent to each VSCU at point 1. Ideally, the disharmony system will restore to harmony state and $f_d=0$, though it is difficult to realize precisely. In general, the disharmony frequency is f_{d2} and $-|f_{d1}|<|f_{d2}|<0$ after point 1. A new frequency control instruction is sent to each VSCU at point 2 before $P_s(t)$ is almost close to $P_{s\text{-lowl}}$. In this way, the control sequences are formed to guarantee $P_s(t)$ be within the upper and lower limits.

In practice, when $P_s(t)$ or $P_r(t)$ satisfies (33) or (34) in the monitoring process, the frequency control instructions are sent to each VSCU.

$$P_s(t)\geqslant P_{s\text{-upl}} \quad \text{or} \quad P_s(t)\leqslant P_{s\text{-lowl}} \tag{33}$$

$$P_r(t)\geqslant P_{r\text{-upl}} \quad \text{or} \quad P_r(t)\leqslant P_{r\text{-lowl}} \tag{34}$$

where $P_{s\text{-upl}}$, $P_{s\text{-lowl}}$, $P_{r\text{-upl}}$, and $P_{r\text{-lowl}}$ are the trigger upper and lower thresholds for issuing frequency control instructions when $P_s(t)$ or $P_r(t)$ exceeds the limits. In Section IV, the upper and lower thresholds are set to 1.2 times and 0.8 times the maximum power transfer capacity of the AC line, respectively.

In summary, Fig. 2 shows that the DOS strategy I needs to directly measure and transmit multiple frequency signals, and its control performance depends on frequency measurement and transmission accuracy.

b) DOS Strategy II: Control Strategy Based on Indirectly Monitoring Line Power

The peak power and average power over the fundamental cycle change significantly, and the amplification effect of peak value will occur under DOCs. Based on the changes, a control strategy based on monitoring oscillation power is proposed in Fig. 4 which consists of four parts.

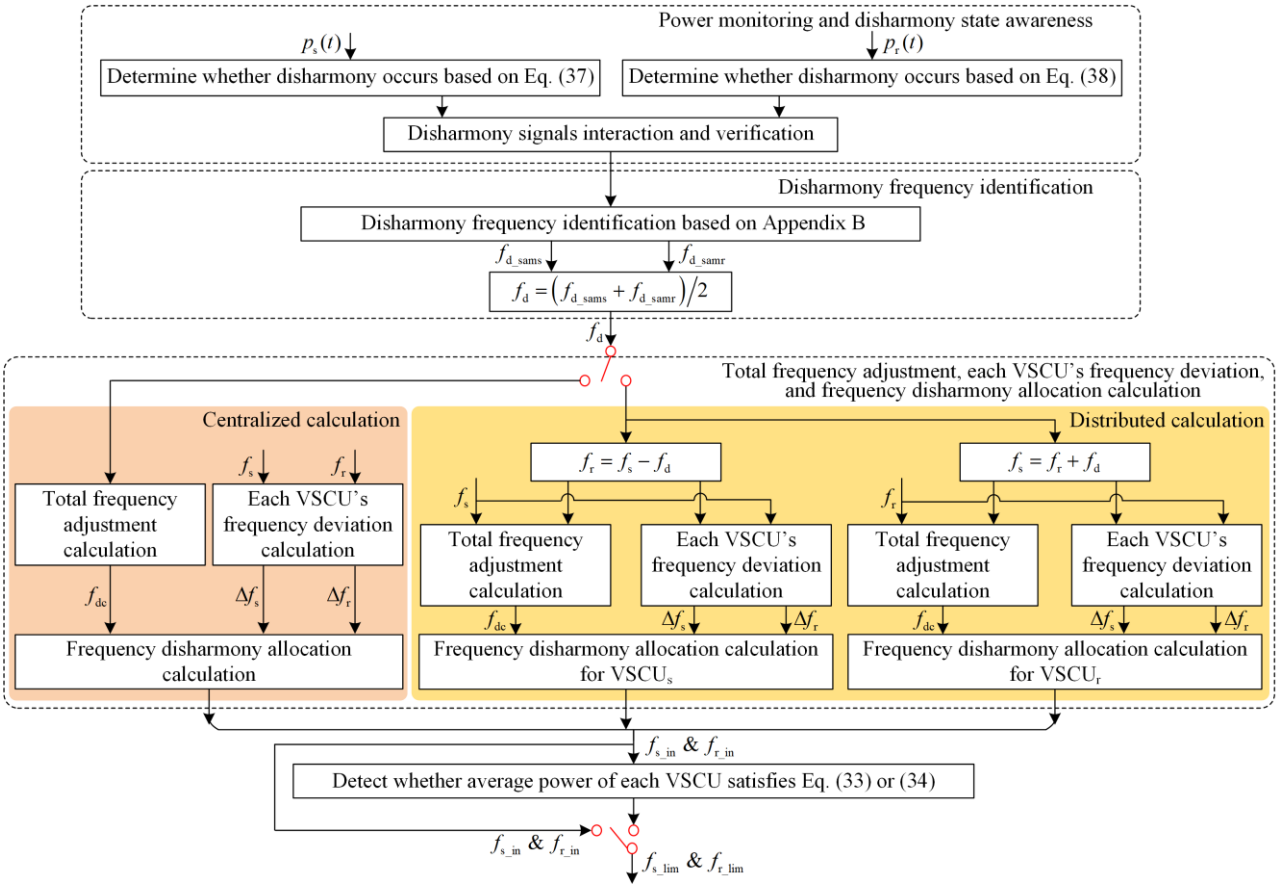

Fig. 4. DOS based on monitoring oscillation power.

Part 1 is about the power monitoring and disharmony state awareness.

First, based on $p_s(t)$ and $p_r(t)$, the average power of $VSCU_s$ and $VSCU_r$ over fundamental cycle T_{sys} are calculated by (35) and (36) denoted as $\bar{P}_s(t)$ and $\bar{P}_r(t)$.

$$\bar{P}_s(t)=\frac{1}{T_{sys}}\int_{t-T_{sys}}^{t}p_s(t)\mathrm{d}t \tag{35}$$

$$\bar{P}_r(t)=\frac{1}{T_{sys}}\int_{t-T_{sys}}^{t}p_r(t)\mathrm{d}t \tag{36}$$

Second, $VSCU_s$ and $VSCU_r$ monitor whether $\bar{P}_s(t)$ and $\bar{P}_r(t)$ satisfy (37) and (38) during the recent T_w, respectively. If either $\bar{P}_s(t)$ or $\bar{P}_r(t)$ satisfies (37) or (38), $VSCU_s$ and $VSCU_r$ enter the disharmony state.

$$\left|\bar{P}_s(t)/P_s(t)\big|_{f_d=0}-1\right|\geqslant\varepsilon_3 \tag{37}$$

$$\left|\bar{P}_r(t)/P_r(t)\big|_{f_d=0}-1\right|\geqslant\varepsilon_4 \tag{38}$$

where ε_3 and ε_4 are the thresholds of power ratios of $\bar{P}_s(t)$ and $\bar{P}_r(t)$ for detecting disharmony. ε_3 and ε_4 can be determined according to the maximum power transfer capacity of the AC line.

A mechanism of interaction and verification between sending and receiving ends is established to ensure the reliability of the results of disharmony state awareness. If any VSCU detects disharmony, the result of detection will be transmitted to the other side for verification. This function is accomplished by the "Disharmony signals interaction and verification" in Fig. 4. When the disharmony signals are verified, the signals for frequency adjustment will be executed by each VSCU.

Part 2 is about the disharmony frequency identification.

The disharmony frequency still denoted as f_d can be identified by the method in Appendix B. The disharmony frequencies, denoted as f_{d_sams} and f_{d_samr}, can be identified based on $P_s(t)$ or the average value of $p_s(t)$, and $P_r(t)$ or the average value of $p_r(t)$, respectively. Finally, the average value of f_{d_sams} and f_{d_samr} is taken as the identification result.

Part 3 is about the total frequency adjustment, each VSCU's frequency deviation, and frequency disharmony allocation calculation.

After disharmony frequency identification, f_{s_in} and f_{r_in} can be determined in the following two ways:

1) Computing mode 1: centralized calculation. Calculate f_{s_in} and f_{r_in} at top-level control center based on Parts 1–3 in DOS strategy I.

2) Computing mode 2: distributed calculation. f_d from the top-level control center is sent to each VSCU. Calculate f_{s_in} or f_{r_in} locally by using the frequency of VSCU on the opposite side and frequency of VSCU from measurement on the local side based on Parts 1–3 in the DOS strategy I.

Part 4 is about the frequency control instruction transmission.

For centralized calculation, frequency control instructions are issued to each VSCU based on Part 4 in DOS strategy I.

For distributed calculation, each VSCU determines whether the average power of VSCU on the opposite side satisfies (37) or (38). If the average power of one VSCU exceeds the limit, VSCUs adjust frequency based on f_{s_in} and f_{r_in}.

In summary, the instantaneous power and average power are used to identify the disharmony frequency in the DOS strategy II. It is still necessary to utilize the measurement signals in Part 3, including f_s, f_r and f_{sys}.

2) DOS Strategy Based on Multiple Means

Other key indicators in Section III.A can be applied to design DOS strategies based on multiple means. For instance, DOS strategy based on multiple means can be designed as a primary and backup fusion, or as a weighted fusion based on the frequency obtained from DOS strategies I and II. In addition, DOS strategies based on the line current can become another control approach. Due to length limitation, they are not introduced further in this paper.

IV. Simulation and Experiment Results

A. Simulation Results of Power Flow

Case studies that simulate disharmony occurrence in the equivalent circuit in Fig. 1 are carried out, and the characteristics of disharmony oscillations are thoroughly analyzed.

1) Line Current and Power Under DOCs

Figure 5 illustrates $i_s(t)$, $I_{sm}(t)$, $p_s(t)$, and the upper and lower envelopes of $p_s(t)$, whereas Table II shows the key parameters of current and power oscillation.

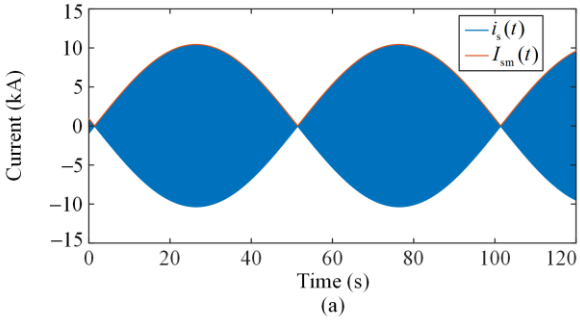

(a)

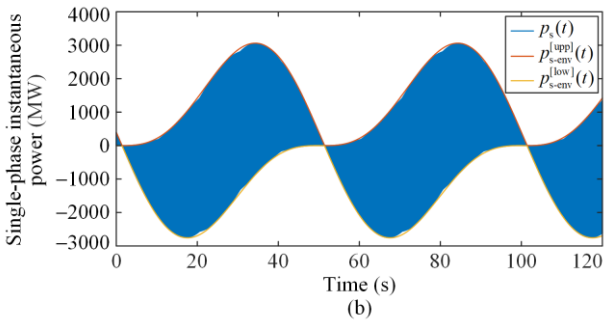

Fig. 5. Power flow under DOC. (a) Single-phase instantaneous current $i_s(t)$ and its peak value $I_{sm}(t)$ of VSCUs. (b) Single-phase instantaneous power $p_s(t)$, and the upper and lower envelopes of $p_s(t)$.

TABLE II
CURRENT PEAK AND POWER PEAK OF VSCUS AND CHARACTERISTIC INDICATORS

Condition	Parameter	Value
Under DOC	Maximum value of single-phase instantaneous current of VSCU$_s$ under DOC (kA)	10.339
	Maximum current peak of line current $I_{sm(max)}$ (kA)	10.438
	Maximum of single-phase instantaneous power of VSCUs under DOC (MW)	3056.412
	Minimum of single-phase instantaneous power of VSCU$_s$ under DOC (MW)	–2744.836
	Maximum of upper envelope of single-phase instantaneous power of VSCU$_s$ $P^{[upp]}_{s\text{-}env(max)}$ (MW)	3061.595
	Minimum of lower envelopes of single-phase instantaneous power of VSCU$_s$ $P^{[low]}_{s\text{-}env(min)}$ (MW)	–2756.548
Under HOC	Current peak of VSCU$_s$ under HOC $I^{[har]}_{sm}$ (kA)	0.933
	Peak value of single-phase instantaneous power of VSCU$_s$ under HOCs $P^{[har]}_{smax}$ (MW)	399.730
Gain	Current peak gain K_{cp}	11.185
	Power peak gain K_{pp}	7.659

As illustrated in Fig. 5 and Table II, the following characteristics of disharmony oscillations can be obtained: 1) The periods of $I_{sm}(t)$ and $p_s(t)$ are 50 s; 2) Disharmony will lead to amplification effect of the line current peak and line power peak; and 3) The amplification degree of the power peak is lower than that of the current peak. Regardless of the degree of amplification, it will have an impact on the power grid security and must thus be taken seriously.

2) Characteristics of Power Transmission and Energy Issues

a) Long Period and Bidirectional Transmission

Figure B1 and Fig. 6 illustrate active power $P_s(t)$ and power factor angle $\theta(t)$, respectively. The periods of the curves are 50 s which is much larger than the fundamental period 0.02 s. The single-phase active power $P_s(t)$ is positive for 26.44 s and negative for 23.56 s during a disharmony period due to the periodicity of $\theta(t)$, demonstrating that disharmony causes reverse power flow.

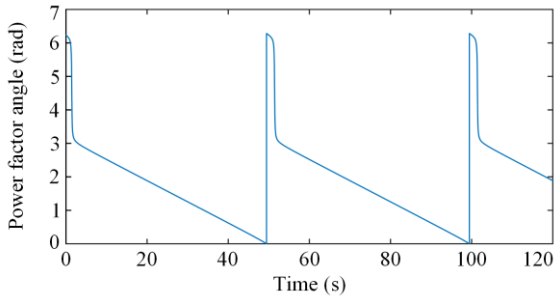

Fig. 6. Power factor angle under DOCs.

b) Total Energy Conservation and Periodic Power

Appendix A shows that the average values of $p_s(t)$ and $P_s(t)$ are equal during the disharmony period. Further, Fig. B2 illustrates that when $|f_d| \leqslant 0.02$ Hz, the average value of $p_s(t)$ or $P_s(t)$ is within the range of [101.366 MW, 101.449 MW] and remains almost unchanged during the disharmony period. The total energy remains unchanged. This characteristic indicates that as long as the amplification effect occurs, the peak reduction effect must occur during the rest of the disharmony period. Therefore, amplification and reduction effects occur in turn in Fig. B1. Based on energy invariant feature, the DOS strategy II is proposed in Section III.B based on total energy conservation.

B. Simulation Results of DOS

This section will verify the two DOS strategies including monitoring disharmony and determining frequency control instructions based on the equivalent circuit model in Fig. 1. The threshold settings are specified in Table III.

Four DOCs are defined as follows.

Case I: Set $f_s = 49.99$ Hz and $f_r = 50.01$ Hz at 0.5 s.

Case II: Set $f_s = 49.99$ Hz and $f_r = 50$ Hz at 0.5 s.

Case III: Set $f_s = 49.995$ Hz and $f_r = 50.005$ Hz at 0.5 s.

Case IV: Set $f_s = 49.99$ Hz and $f_r = 49.99$ Hz at 0.5 s.

Figure 7 shows the active power of each VSCU, where the power magnitude exceeds both the upper and lower limits. Subsequently, two DOS strategies are verified.

TABLE III
THRESHOLD PARAMETER OF THE TWO DOS STRATEGIES

Parameter	Value
Trigger upper threshold of $P_s(t)$ for issuing frequency control instructions $P_{s\text{-upl}}$ (MW)	1.2×204.5
Lower threshold of $P_s(t)$ for issuing frequency control instructions $P_{s\text{-lowl}}$ (MW)	0.8×204.5
Trigger upper threshold of $P_r(t)$ for issuing frequency control instructions $P_{r\text{-upl}}$ (MW)	1.2×201.2
Lower threshold of $P_r(t)$ for issuing frequency control instructions $P_{r\text{-lowl}}$ (MW)	0.8×201.2
Threshold value of disharmony frequency ε_1 (Hz)	0.001
Threshold value of disharmony frequency ε_2 (Hz)	0.001
Thresholds of power ratios of the average power of $VSCU_s$ over fundamental cycle ε_3 (Hz)	0.05
Thresholds of power ratios of the average power of $VSCU_r$ over fundamental cycle ε_4 (Hz)	0.05
Sampling period of active power t_{sam} (s)	0.1
Constant term in expression of active power at sending end P_{Es} (MW)	101.41
Amplitude of the sine term in expression of active power at send end P_{Ms} (MW)	112.34
Constant term in expression of active power at receiving end P_{Er} (MW)	937.52
Amplitude of the sine term in expression of active power at receiving end P_{Mr} (MW)	112.37

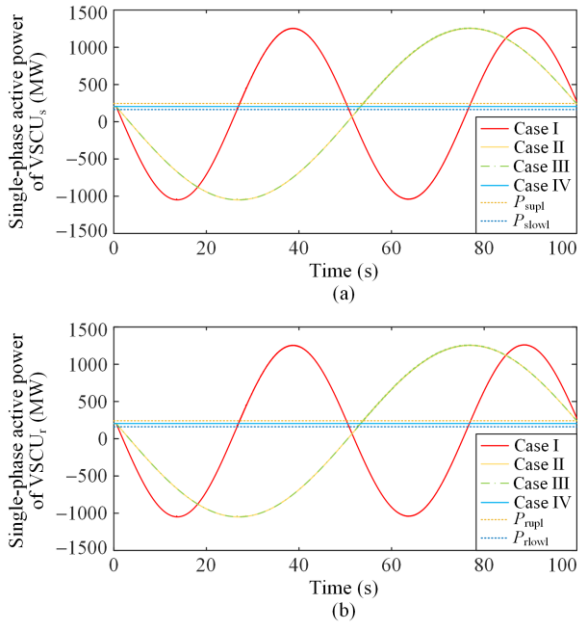

Fig. 7. Active power in Cases I–IV. (a) Single-phase active power of $VSCU_s$. (b) Single-phase active power of $VSCU_r$.

1) DOS Strategy I

Figures 8 and 9 show the active power and frequency of each VSCU. P_s exceeds the lower limit at around 0.796 s in Case I while P_r exceeds the lower limit at around 0.794 s, 1.076 s and 1.076 s in Case I, II and III, respectively. In Cases I–III, frequency control instructions are issued to each VSCU when P_r exceeds the lower limit. In Case IV, frequency control instructions are issued to each VSCU upon persistent detection of frequency disharmony.

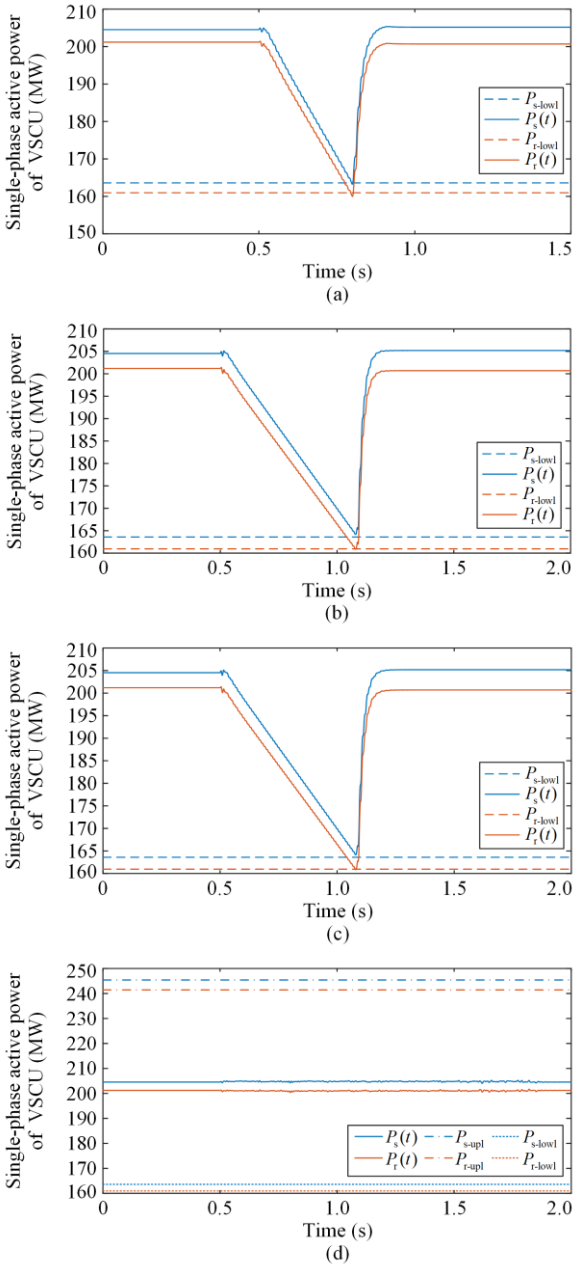

Fig. 8. Active power of each VSCU in Cases I–IV. (a) Case I. (b) Case II. (c) Case III. (d) Case IV.

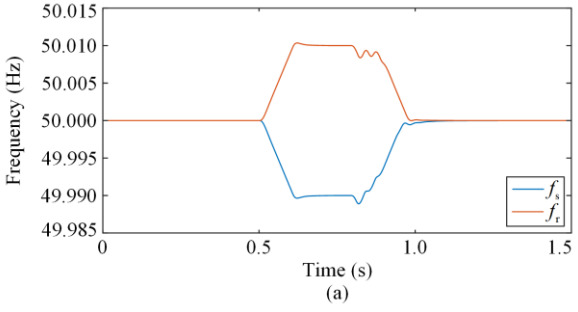

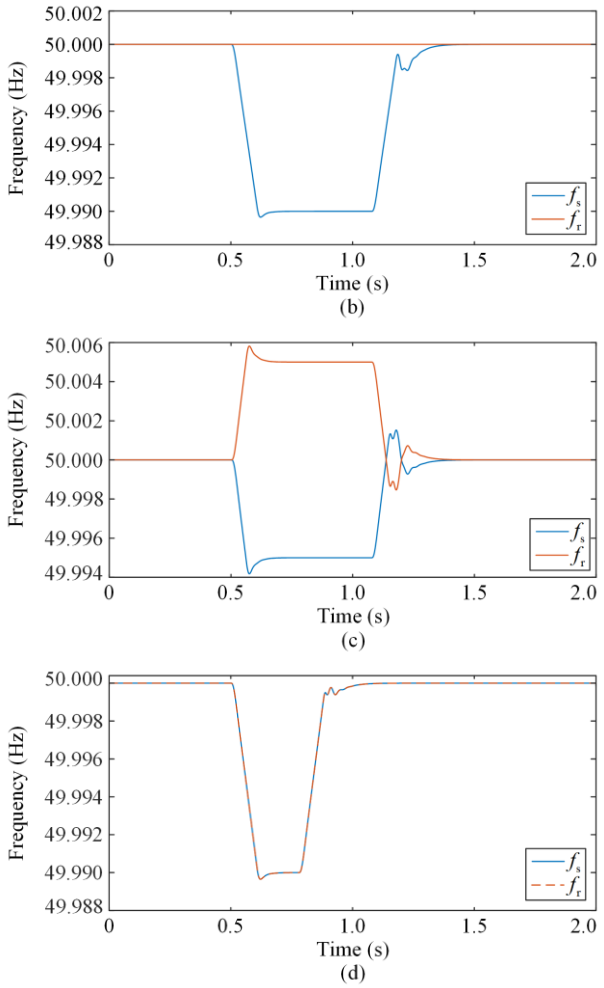

Fig. 9. Frequency of each VSCU in Cases I–IV. (a) Case I. (b) Case II. (c) Case III. (d) Case IV.

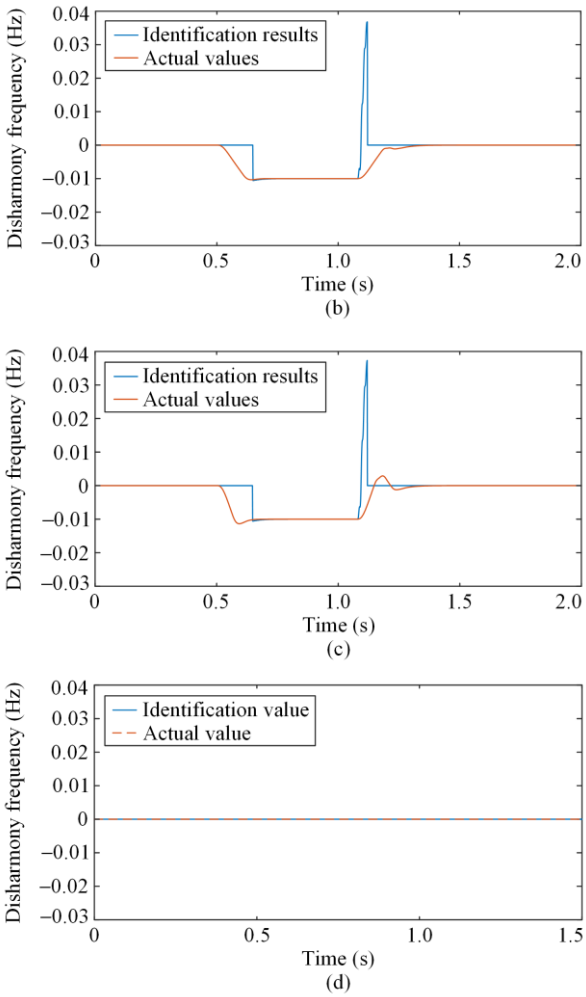

Fig. 10. Identification results and actual values of disharmony frequency in Cases I–IV. (a) Case I. (b) Case II. (c) Case III. (d) Case IV.

2) DOS Strategy II

Identify f_d based on the line power when either $\bar{P}_s(t)$ or $\bar{P}_r(t)$ satisfies (37) or (38). The results are shown in Fig. 10.

Figures 11 and 12 show the active power and frequency of each VSCU in Cases I–IV. P_s exceeds the lower limit at around 0.796 s in Case I while P_r exceeds the lower limit at around 0.794 s, 1.076 s and 1.076 s in Case I, II and III, respectively. Based on the identification results, frequency control instructions are issued to each VSCU.

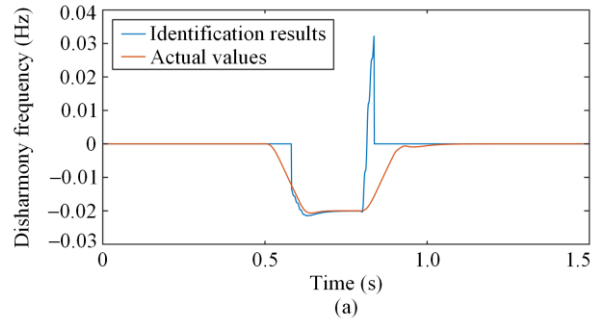

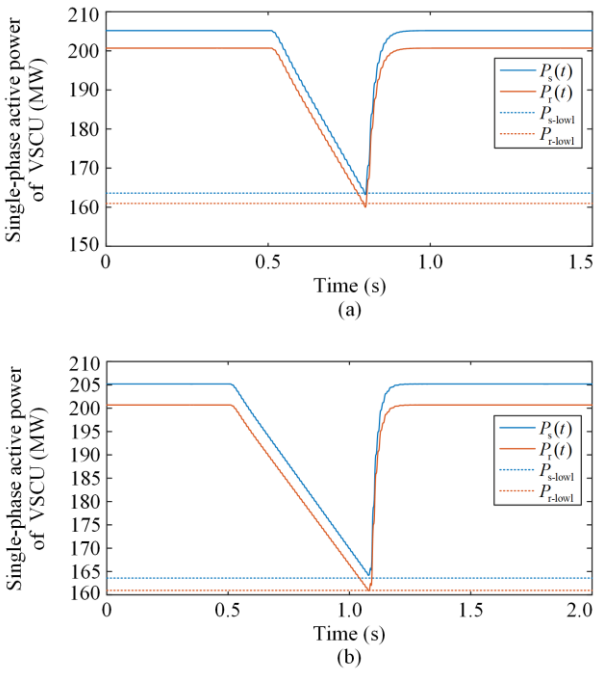

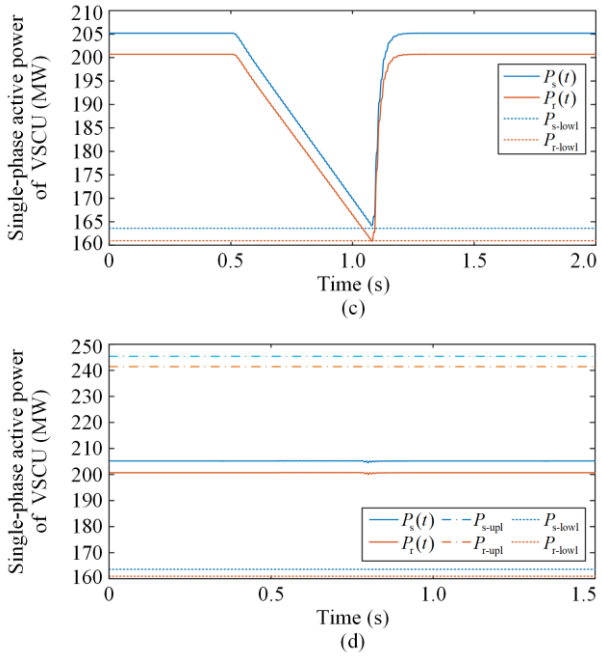

Fig. 11. Active power each VSCU in Cases I–IV. (a) Case I. (b) Case II. (c) Case III. (d) Case IV.

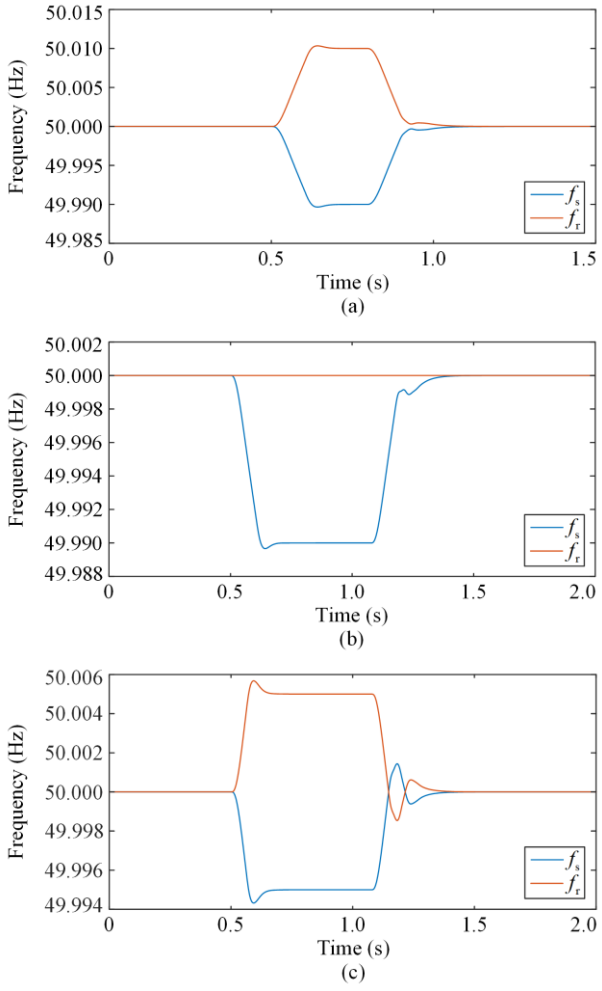

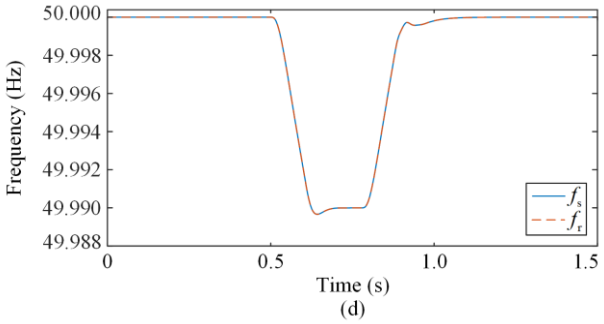

Fig. 12. Frequency of each VSCU in Case I–IV. (a) Case I. (b) Case II. (c) Case III. (d) Case IV.

In summary, Figs. 9 and 12 show that both DOS strategies I and II can control the line power near the homodyne operating level.

3) Noise Impact

To validate the impact of noises on control performance, a random sequence is added to f_s and f_r from wide area measurement system in Fig. 1 to simulate noises. The sequence follows a (0, 1)×0.001 uniform distribution. Figures 13 and 14 show the performance of DOS strategies I and II under noisy condition in Case I. It demonstrates that the control strategy has noise suppression capability and the suppression effect is not affected by the noise.

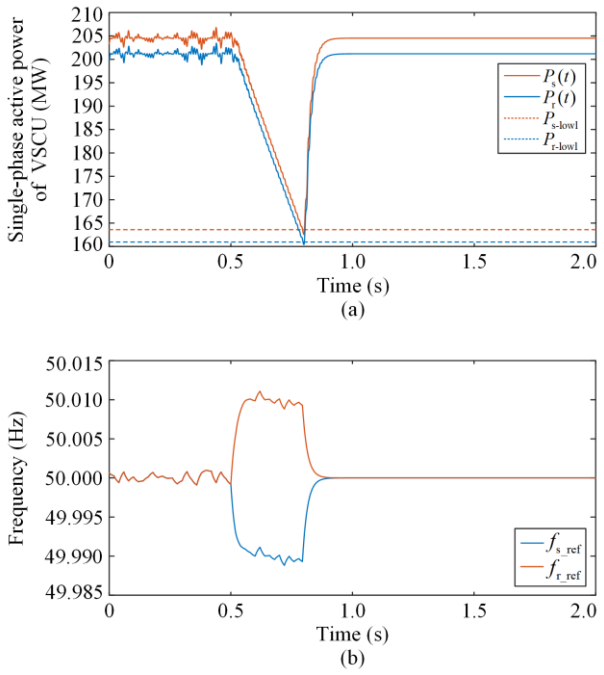

Fig. 13. Performance of DOS strategy I under noisy condition in Case I. (a) Active power of each VSCU. (b) Frequency reference of each VSCU.

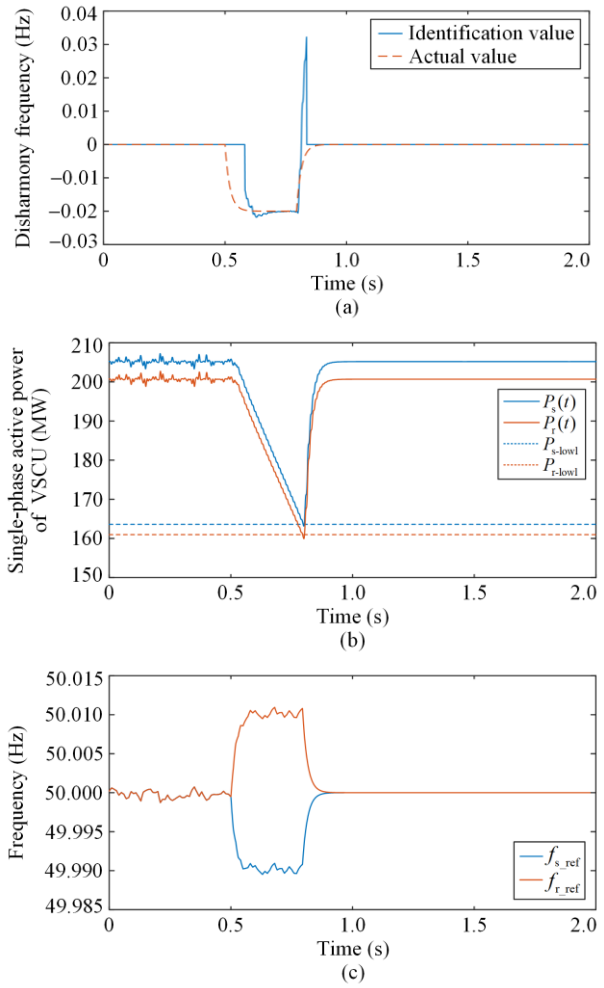

Fig. 14. Performance of DOS strategy II under noisy condition in Case I. (a) Identification results and actual values of disharmony frequency. (b) Active power of each VSCU. (c) Frequency reference of each VSCU.

4) Comparison of Two Strategies

Comparison of the two strategies shows that key distinctions between DOS strategies I and II include the following two aspects.

1) DOS Strategy II exhibits superior detection capability over DOS Strategy I in identifying frequency disharmony occurrences. Section II.C and IV.A show that disharmony causes amplification or reduction of power under DOCs. The order of magnitude of power variation is bigger than the order of magnitude of disharmony frequency. Monitoring power variation is simpler than monitoring disharmony frequency in DOS strategy I.

2) DOS strategy I requires fewer measurement signals than DOS strategy II in frequency deviation and frequency disharmony allocation calculation. DOS strategy I directly utilizes each VSCU's frequency or disharmony frequency. In contrast, DOS strategy II mainly relies on instantaneous power sampling signals or the average power to identify f_{d}. Additionally, it requires the frequency measurement signals, including f_{s}, f_{r} and f_{sys} in each VSCU's frequency deviation and frequency disharmony allocation calculation.

Based on the control strategy schemes and aforementioned distinctions, the application scenarios for DOS strategies I and II are outlined below.

1) DOS strategy I is more suitable for operating in centralized control mode and monitoring signals solely consist of each VSCU's frequency.

2) DOS strategy II is more suitable for operating in either distributed or centralized control modes, depending on whether computational resources are deployed on the VSCU side. In addition, it is more effective in scenarios with minimal variations of $\left|f_{\mathrm{r}}-f_{\mathrm{s}}\right|$.

V. Conclusion

For AC transmission line with two disharmonized VSCUs, this paper analyzes the characteristics of disharmony oscillation and proposes solutions. The conclusions drawn from the analysis are given below.

1) Under DOCs, disharmony oscillations including current and active power oscillations occur at power grid side, whose periods are generally long. Meanwhile, peak amplification effect of the line current and power occurs, thereby threatening the stable operation of the power grid.

2) The key parameters and characteristic indicators are proposed, such as frequency difference, line current and line power, etc. They can provide important information for online monitoring disharmony oscillations.

3) The DOS strategies respectively based on directly monitoring the frequency difference and indirectly monitoring line power are proposed. While two strategies exhibit subtle differences in application scenarios, both demonstrate the capability to rapidly adjust line power flow to harmony states within a short timeframe when grid line power exceeds operational limits.

Appendix A

This section talks about the relationship between $P_{\mathrm{s}}(t)$ and the average value of $p_{\mathrm{s}}(t)$ during one disharmony period.

Let $T_{\mathrm{d}}=nT_{\mathrm{sys}}$, and the average value $\bar{P}_{\mathrm{s}}(T_{\mathrm{d}})$ of $p_{\mathrm{s}}(t)$ with $t\in[0,\ T_{\mathrm{d}}]$ is:

$$\bar{P}_{\mathrm{s}}(T_{\mathrm{d}})=\frac{1}{T_{\mathrm{d}}}\int_0^{T_{\mathrm{d}}}p_{\mathrm{s}}(t)\mathrm{d}t=\frac{1}{nT_{\mathrm{sys}}}\sum_{i=1}^{n}\int_{(i-1)T_{\mathrm{sys}}}^{iT_{\mathrm{sys}}}p_{\mathrm{s}}(t)\mathrm{d}t=\frac{1}{nT_{\mathrm{sys}}}\sum_{i=1}^{n}T_{\mathrm{sys}}\bar{P}_{\mathrm{s}}\left(iT_{\mathrm{sys}}\right)=\frac{1}{n}\sum_{i=1}^{n}\bar{P}_{\mathrm{s}}\left(iT_{\mathrm{sys}}\right)\tag{A1}$$

where $\bar{P}_s\left(iT_{sys}\right)$ is the average value of $p_s(t)$ when $t\in\left[(i-1)T_{sys},iT_{sys}\right]$; $\bar{P}_s\left(iT_{sys}\right)$ is the same as the value of $P_s(t)$ when $t=iT_{sys}$.

Thus, the average value of $P_s(t)$ when $t\in\left[0,\ T_d\right]$ is:

$$\frac{1}{T_d}\int_0^{T_d}P_s(t)\mathrm{d}t=\frac{1}{nT_{sys}}\sum_{i=1}^{n}\int_{(i-1)T_{sys}}^{iT_{sys}}P_s(t)\mathrm{d}t=\frac{1}{nT_{sys}}\sum_{i=1}^{n}T_{sys}\bar{P}_s\left(iT_{sys}\right)=\frac{1}{n}\sum_{i=1}^{n}\bar{P}_s\left(iT_{sys}\right) \tag{A2}$$

Equations (A1) and (A2) show that:

$$\frac{1}{T_d}\int_0^{T_d}p_s(t)\mathrm{d}t=\frac{1}{T_d}\int_0^{T_d}P_s(t)\mathrm{d}t=\bar{P}_s(T_d) \tag{A3}$$

That is, the average value of $p_s(t)$ and the average value of $P_s(t)$ are equal for $t\in[0,\ T_d]$.

APPENDIX B

This section talks about the sampling frequency calculation and disharmony frequency identification.

A. Sampling Frequency Calculation

The error of each VSCU's frequency measurement does not exceed 0.01 Hz [38], and $|f_d|\leqslant 0.02$ Hz. The sampling frequency of $P_s(t)$ is larger than or equal to $2|f_d|$ based on the sampling theorem. The sampling cycle of $P_s(t)$ will be from 2.0 s to 5.0 s, if the sampling frequency of $P_s(t)$ is enlarged by 5 to 10 times on this basis. Therefore, the sample cycle of $P_s(t)$ is set as 0.1 s in case studies, and is sufficient to meet the engineering accuracy requirements.

B. Disharmony Frequency Identification

Based on the parameters in Table I, Fig. B1 shows the active power $P_s(t)$ with $f_d=0.02$ Hz.

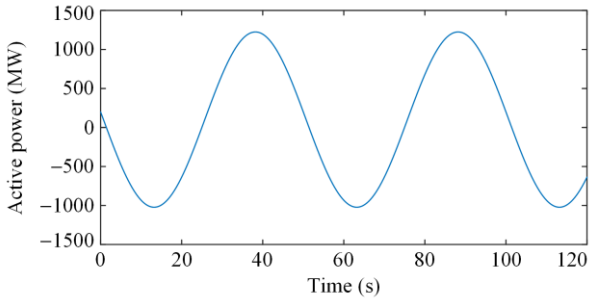

Fig. B1. Single-phase active power.

From Fig. B1, $P_s(t)$ can be approximated by:

$$P_s(t)=P_E+P_M\sin\left(\omega_d t+\zeta\right) \tag{B1}$$

where the constant term P_E is the average value of $P_s(t)$ over one disharmony period; P_M is the amplitude of the sine term; and ζ is the initial phase of the sine term.

In addition, Fig. B2 shows the average and maximum values of $P_s(t)$ and $P_r(t)$ over a disharmony period with different disharmony frequencies.

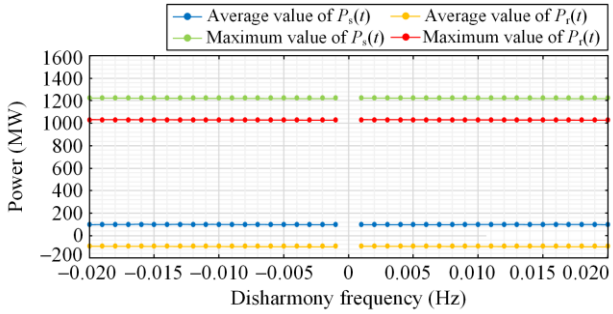

Fig. B2. Average and maximum values of $P_s(t)$ and $P_r(t)$ over disharmony cycle with different disharmony frequencies.

The average and maximum values of $P_s(t)$ and $P_r(t)$ are almost constant during the disharmony period when $|f_d|\leqslant 0.02$ Hz. P_E and P_M in (B1) can be treated as fixed values corresponding to HOC according to Fig. B2. At least two sampling points on the single-phase active power curve need to be sampled to identify f_d. When the sampling period of the $P_s(t)$ is t_{sam}, the kth and $(k+1)$th sampling points of $P_s(t)$ are:

$$P_s(k)=P_E+P_M\sin\left(\omega_d k t_{sam}+\zeta\right) \tag{B2}$$

$$P_s(k+1)=P_E+P_M\sin\left[\omega_d\left(k+1\right)t_{sam}+\zeta\right] \tag{B3}$$

Solving (B2) and (B3) yields:

$$\begin{cases}\omega_d=\dfrac{\arcsin\dfrac{P_s(k+1)-P_E}{P_M}-\arcsin\dfrac{P_s(k)-P_E}{P_M}}{t_{sam}}\\ \zeta=\arcsin\dfrac{P_s(k)-P_E}{P_M}-k\left(\arcsin\dfrac{P_s(k+1)-P_E}{P_M}-\arcsin\dfrac{P_s(k)-P_E}{P_M}\right)\end{cases} \tag{B4}$$

ACKNOWLEDGMENT

Not applicable.

AUTHORS' CONTRIBUTIONS

Qiyi Yu: conceptualization, investigation, writing original draft, methodology, software, and formal analysis. Yi Tang: writing—writing review, editing, supervision, funding acquisition, and formal analysis. Both authors read and approved the final manuscript.

FUNDING

This work is supported by the National Natural Science Foundation of China (No. 52261145704 and No. 52377085).

AVAILABILITY OF DATA AND MATERIALS

Not applicable.

DECLARATIONS

Competing interests: The authors declare that they have no known competing financial interests or personal relationships that could have appeared to influence the work reported in this article.

AUTHORS' INFORMATION

Qiyi Yu received the B.S. degree in electrical engineering from Shandong University, Jinan, China, in 2017, and the M.S. degree from Nanjing Normal University, Nanjing, China, in 2020. She is currently pursuing the Ph.D. degree at the School of Electrical Engineering, Southeast University, Nanjing, China. Her main research interest includes wide-frequency oscillation.

Yi Tang received the B.E., M.E., and Ph.D. degrees from Harbin Institute of Technology, Harbin, China, in 2000, 2002, and 2006, respectively. He is currently a professor at the School of Electrical Engineering, Southeast University, Nanjing, China. His research interests include smart grid, power system security, power system stability analysis, renewable energy systems, and cyber-physical systems.

REFERENCES

[1] M. Zhang, Y. Han, and Y. Liu *et al.*, "Multi-timescale modeling and dynamic stability analysis for sustainable microgrids: state-of-the-art and perspectives," *Protection and Control of Modern Power Systems*, vol. 9, no. 3, pp. 1-35, May 2024.

[2] Z. Zeng, J. Zhao, and S. Zhang *et al*., "Sensitivity analysis of different controller parameters on the stability of the weak-grid-tied interlinking VSC," *Protection and Control of Modern Power Systems*, vol. 10, no. 1, pp. 40-51, Jan. 2025.

[3] S. Li, H. Wang, and Y. Huang *et al.* (2025, May), "Small-signal stability and parameter regions analysis of grid-forming PV system based on matching control," *Power System Protection and Control*, [Online]. Available: https://doi.org/10.19783/j.cnki.pspc.241744 (in Chinese)

[4] L. Kong, C. Wu, and J. Xu *et al*., "Enhanced DC-link voltage synchronization control for grid-forming photovoltaic systems considering PV power dynamics and grid strength adaptability," *IEEE Transactions on Energy Conversion*, vol. 40, no. 3, pp. 2610-2623, Sept. 2025.

[5] C. Sun, N. Wang, and Y. Ding *et al*., "A fast estimation of the intrinsic low-frequency oscillation modes of modular multilevel converter based on AC impedance modeling," *IEEE Transactions on Industrial Electronics*, vol. 72, no. 5, pp. 4412-4423, May 2025.

[6] L. Zhao, Z. Jin, and X. Wang, "Small-signal synchronization stability of grid-forming converters with regulated dc-link dynamics," *IEEE Transactions on Industrial Electronics*, vol. 70, no. 12, pp. 12399-12409, Dec. 2023.

[7] X. Jiang, H. Yi, and Y. Li *et al*., "Low-frequency oscillation damping of grid-forming STATCOMs with phase-compensated DC-link voltage synchronization," *IEEE Transactions on Power Electronics*, vol. 40, no. 2, pp. 2860-2873, Feb. 2025.

[8] X. Zhou, S. Cheng, and X. Wu *et al*., "Influence of photovoltaic power plants based on VSG technology on low frequency oscillation of multi-machine power systems," *IEEE Transactions on Power Delivery*, vol. 37, no. 6, pp. 5376-5384, Dec. 2022.

[9] Y. Ma, J. Xu, and C. Gao *et al*., "Low-frequency oscillations and resonance analysis of VSG-controlled PMSG-based wind generation systems," *Journal of Modern Power Systems and Clean Energy*, vol. 13, no. 1, pp. 115-127, Jan. 2025.

[10] Y. Yu, S. K. Chaudhary, and G. D. A. Tinajero *et al*., "Active damping for dynamic improvement of multiple grid-tied virtual synchronous generators," *IEEE Transactions on Industrial Electronics*, vol. 71, no. 4, pp. 3673-3683, Apr. 2024.

[11] T. Xue, J. Zhang, and S. Bu, "Inter-area oscillation analysis of power system integrated with virtual synchronous generators," *IEEE Transactions on Power Delivery*, vol. 39, no. 3, pp. 1761-1773, Jun. 2024.

[12] N. Mohammed, M. H. Ravanji, and W. Zhou *et al*., "Online grid impedance estimation-based adaptive control of virtual synchronous generators considering strong and weak grid conditions," *IEEE Transactions on Sustainable Energy*, vol. 14, no. 1, pp. 673-687, Jan. 2023.

[13] W. Yan, S. Shah, and V. Gevorgian *et al*., "On the low risk of SSR in type III wind turbines operating with grid-forming control," *IEEE Transactions on Sustainable Energy*, vol. 15, no. 1, pp. 443-453, Jan. 2024.

[14] Z. Zhou, S. Pugliese, and M. Langwasser *et al*., "Subsynchronous damping by battery storage system in grid-forming control," *IEEE Transactions on Power Electronics*, vol. 39, no. 4, pp. 4173-4186, Apr. 2024.

[15] F. Puricelli, P. Rault, and C. Cardozo *et al*., "Analysis and damping of grid-forming converters interactions in bipolar HVDC connections using a coordinate transformation approach," *International Journal of Electrical Power & Energy Systems*, vol. 165, pp. 1-11, Apr. 2025.

[16] H. Wu and X. Wang, "Small-signal modeling and controller parameters tuning of grid-forming VSCs with adaptive virtual impedance-based current limitation," *IEEE Transactions on Power Electronics*, vol. 37, no. 6, pp. 7185-7199, Jun. 2022.

[17] F. Zhao, X. Wang, and T. Zhu, "Power dynamic decoupling control of grid-forming converter in stiff grid,"

IEEE Transactions on Power Electronics, vol. 37, no. 8, pp. 9073-9088, Aug. 2022.

[18] W. Yan, S. Shah, and V. Gevorgian *et al*., "On the low risk of SSR in type III wind turbines operating with grid-forming control," *IEEE Transactions on Sustainable Energy*, vol. 15, no. 1, pp. 443-453, Jan. 2024.

[19] P. Huang, and L. Vanfretti, "Multi-tuned narrowband damping for suppressing MMC high-frequency oscillations," *IEEE Transactions on Power Delivery*, vol. 38, no. 6, pp. 3804-3819, Dec. 2023.

[20] T. Xu, H. Shu, and H. Feng *et al*., "High frequency stability analysis and oscillation suppression strategy for an MMC considering link delays", *Power System Protection and Control*, vol. 53, no. 8, pp. 58-70, May 2025. (in Chinese)

[21] L. Lin, Q. Zeng, and J. Zhu *et al*., "High-frequency oscillation mechanism analysis and suppression strategy of grid-forming control MMC-HVDC," *IEEE Transactions on Power Delivery*, vol. 38, no. 3, pp. 1588-1600, Jun. 2023.

[22] F. Dai, S. Liu, and G. Wang *et al*., "Coordinated suppression strategies for passive and active resonances of the MMC-HVDC AC-side system on the medium- and high-frequency bands," *IET Generation, Transmission & Distribution*, vol. 17, no. 13, pp. 2963-2977, Jan. 2023.

[23] S. Chen, Y. Sun, and H. Han *et al*., "A modified VSG control scheme with virtual resistance to enhance both small-signal stability and transient synchronization stability," *IEEE Transactions on Power Electronics*, vol. 38, no. 5, pp. 6005-6014, May 2023.

[24] C. Fang, L. Mu, and Z. Wang *et al*., "Analysis of grid-forming IIDG's transient- and steady-state fault model," *IEEE Transactions on Smart Grid*, vol. 13, no. 2, pp. 1187-1199, Mar. 2022.

[25] B. Liu, X. Xiang, and Y Li *et al*., "On the transient overcurrent mechanism of grid forming converter in fault recovery stage," *IEEE Transactions on Power Electronics*, vol. 39, no. 10, pp. 12163-12169, Oct. 2024.

[26] A. Arjomandi-Nezhad, Y. Guo, and B. C. Pal *et al*., "A model predictive approach for enhancing transient stability of grid-forming converters," *IEEE Transactions on Power Systems*, vol. 39, no. 5, pp. 6675-6688, Sept. 2024.

[27] P. Sun, Z. Tian, and X. Zha *et al*., "Hybrid power synchronization based transient stability enhanced control for grid-forming inverters under symmetrical grid fault," *IEEE Transactions on Power Electronics*, vol. 40, no. 2, pp. 2780-2796, Feb. 2025.

[28] W. Si and J. Fang, "Transient stability improvement of grid-forming converters through voltage amplitude regulation and reactive power injection," *IEEE Transactions on Power Electronics*, vol. 38, no. 10, pp. 12116-12125, Oct. 2023.

[29] G. Wang, L. Fu, and Q. Hu *et al*., "Transient synchronization stability of grid-forming converter during grid fault considering transient switched operation mode," *IEEE Transactions on Sustainable Energy*, vol. 14, no. 3, pp. 1504-1515, Jul. 2023.

[30] K. G. Saffar, S. Driss, and F. B. Ajaei, "Impacts of current limiting on the transient stability of the virtual synchronous generator," *IEEE Transactions on Power Electronics*, vol. 38, no. 2, pp. 1509-1521, Feb. 2023.

[31] Y. Xue, Z. Zhang, and G. Wang *et al*. (2024, Jul.), "Transient stability analysis between SG and grid-forming VSCs with current saturation control considering backward-swing dynamics", *CSEE Journal of Power and Energy Systems*, [Online]. Available: https://ieeexplore.ieee.org/document/10609294

[32] Y. Liu, H. Geng, and M. Huang *et al*., "Dynamic current limiting of grid-forming converters for transient synchronization stability enhancement," *IEEE Transactions on Industry Applications*, vol. 60, no. 2, pp. 2238-2248, Mar. 2024.

[33] P. Ge, C. Tu, and F. Xiao *et al*., "Design-oriented analysis and transient stability enhancement control for a virtual synchronous generator," *IEEE Transactions on Industrial Electronics*, vol. 70, no. 3, pp. 2675-2684, Mar. 2023.

[34] S. Chen, Y. Sun, and X. Hou *et al*., "Quantitative parameters design of VSG oriented to transient synchronization stability," *IEEE Transactions on Power Systems*, vol. 38, no. 5, pp. 4978-4981, Sept. 2023.

[35] L. Huang, C. Wu, and D. Zhou *et al*., "A power-angle-based adaptive overcurrent protection scheme for Grid-Forming inverter under large grid disturbances," *IEEE Transactions on Industrial Electronics*, vol. 70, no. 6, pp. 5927-5936, Jun. 2023.

[36] Q. Yu and Y. Tang, "Mechanism analysis of power oscillation caused by disharmony of voltage source controlled-units at both sides of transmission line," *Proceedings of the CSEE*, vol. 44, no. 15, pp. 5908-5921, Aug. 2024. (in Chinese)

[37] Q. Yu and Y. Tang, "Characteristic analysis of power oscillations caused by disharmony among voltage-source-controlled units in three-terminal local power grid," *Journal of Modern Power Systems and Clean Energy*, vol. 12, no. 4, pp. 1295-1308, Jul. 2024.

[38] Power Quality-Allowable Deviation of Power System Frequency, GB/T 15945-2008, 2008.

[39] C. A. Savalov, "Overview of the unified power system operation modes in the Soviet Union & analytical methods for electrotechnical problems," in *Operation Mode of the Unified Power System*, Beijing, China: Hydropower Press, 1988, pp. 94-119.